

# Color Transparency in Semi-Inclusive Electroproduction of $\rho$ Mesons

L. Frankfurt<sup>1</sup>, G.A Miller<sup>2</sup>, M. Strikman<sup>3</sup>

<sup>1</sup> *Tel Aviv University, Tel Aviv, Israel*

<sup>2</sup> *University of Washington, Seattle, WA 98195-1560*

<sup>3</sup> *Pennsylvania State University, University Park, PA 16802*

(Dated: October 30, 2018)

We study the electroproduction of rho mesons in nuclei at intermediate energies, deriving a treatment of the energy lost by the rho in each step of multiple-scattering. This enables a close match between calculations and the experimental kinematic conditions. A standard Glauber calculation is presented, and then the effects of color-transparency are included. The influence of poor experimental resolution on the extracted transparency is assessed. The effects of rho meson decay inside the nucleus are examined, and are typically about 5% at most. This effect disappears rapidly as  $Q^2$  increases from about 1 to 3 GeV<sup>2</sup>, causing a rise in the transparency that is not attributable to color transparency. The size of color transparency effects for C and Fe nuclei is studied for values of  $Q^2$  up to 10 GeV<sup>2</sup>. The detailed results depend strongly on the assumed value of the  $\rho N$  cross section. The overall effects of color transparency are greater than about 10 % for both nuclear targets if  $Q^2$  is greater than about 5 GeV<sup>2</sup>.

PACS numbers: 24.85.+p,25.30.Mr,11.80.-m,12.38.Qk,13.60.-r

Keywords: color transparency, vector meson, electroproduction, nuclear dependence

## I. INTRODUCTION

In the special situation of high-momentum-transfer coherent processes the strong interactions between hadrons and nuclei can be extinguished, causing shadowing to disappear and the nucleus to become quantum-mechanically transparent. This phenomenon is known as color transparency [1, 2, 3]. In more technical language, color transparency is the vanishing of initial and final-state interactions, predicted by QCD to occur in high-momentum-transfer quasi-elastic nuclear reactions. In these reactions, the scattering amplitudes consist of a sum of terms involving different intermediate states and the same final state. Thus one adds different contributions to obtain the scattering amplitude. Under such conditions the effects of gluons emitted by small color-singlet systems tend to cancel [5] and could nearly vanish. Thus color transparency is also known as color coherence.

The important dynamical question is whether or not small color-singlet systems, often referred to as point-like configurations (PLC's), are produced as intermediate states in high momentum transfer reactions. Perturbative QCD predicts that a PLC is formed in many two-body hadronic processes at very large momentum transfer [1, 6]. However, PLC's can

also be formed under non-perturbative dynamics [7, 8]. Therefore measurements of color transparency are important for clarifying the dynamics of bound states in QCD.

Observing color transparency requires that a PLC is formed and that the energies are high enough so that the PLC does not expand completely to the size of a physical hadron while traversing the target [9, 10, 11]. The frozen approximation must be valid.

A direct observation of high-energy color transparency in the  $A$ -dependence of diffractive di-jet production by pions was reported in [12]. The results were in accord with the prediction of [13]. See also [14]. Evidence for color transparency (small hadronic cross-sections) has been observed in other types of processes, also occurring at high energy: in the  $A$ -dependence of  $J/\psi$  photoproduction [15], in the  $Q^2$ -dependence of the  $t$ -slope of diffractive  $\rho^0$  production in deep inelastic muon scattering (where  $Q^2$  is the invariant mass of the virtual photon and  $t$  denotes the negative square of the momentum transfer from the virtual photon to the target proton), and in the energy and flavor dependences of vector meson production in  $ep$  scattering at HERA [16]. For all of these processes the energy is high enough so that the produced small-size configuration does not expand significantly as it makes its way out of the nucleus.

At lower energies expansion effects do occur. Experimental studies of high momentum transfer processes in  $(e, e'p)$  and  $(p, pp)$  reactions have so far failed to produce convincing evidence of color transparency [17, 18, 19, 20]. First data on the reaction  $A(p, 2p)$  at large scattering angles were obtained at BNL. They were followed by the dedicated experiment EVA. The final results of EVA [18] can be summarized as follows. An eikonal approximation calculation agrees with data for  $p_p=5.9$  GeV/c, and the transparency increases significantly for momenta up to about  $p_p=9$  GeV/c. Thus it seems that momenta of the incoming proton  $\sim 10$  GeV are sufficient to significantly suppress expansion effects. Therefore one can use proton projectiles with energies above  $\sim 10$  GeV to study other aspects of the strong interaction dynamics. But the observed drop in transparency for values of  $p_p$  ranging from 11.5 to 14.2 GeV/c represents a problem for all current models, including [21, 22, 23, 24, 25] because of its broad range in energy. This suggests that leading-power quark-exchange mechanism for elastic scattering dominates only at very large energies.

It is natural to expect that it is easier to observe color transparency for the interaction/production of mesons than for baryons because only two quarks have to come close together. A high resolution pion production experiment recently reported evidence for the onset of CT [26] at Jefferson Laboratory in the process  $eA \rightarrow e\pi^+A^*$ . The pion momentum was chosen to be equal to that of the virtual photon,  $\vec{p}_\pi \parallel \vec{q}$  to minimize the importance of elastic rescattering effects. The coherence length defined as the distance between the point where  $\gamma^*$  converted to a  $q\bar{q}$  of invariant mass  $M_{q\bar{q}}$  and where  $q\bar{q}$  interacts with a nucleon -  $|l_{in}| = 2q_0/(Q^2 + M_{q\bar{q}}^2)$ , corresponding to the longitudinal distance between the point where  $\gamma^*$  knocks out a  $q\bar{q}$  pair from the nucleon and the nucleon center, is small for the kinematics of [26], can take on both positive and negative values, and varies weakly with  $Q^2$ . This simplifies the interpretation of the  $Q^2$  dependence of the transparency as compared with the case of small  $x$  where  $l_{in}$  becomes comparable to the size of the nucleus. The experimental results agree well with predictions of [27] and [28].

Does the observation of color transparency in the pion experiments imply that the effect should be observed in the electroproduction of rho mesons? Answering this question is the aim of the present paper, stimulated by the existence of and the expected imminent publication

of a Jlab experiment led by Hafidi[29]. The nuclear targets were the deuteron,  $^{12}\text{C}$  and  $^{56}\text{Fe}$ . They made careful measurements with various experimental cuts. To avoid the effects of resonances the virtual photon-proton cm energy  $W$  was taken as  $W > 2$  GeV, with a range between 2 and 3.1 GeV. To ensure that the reaction process was diffractive, the momentum transfer variable  $t$  was restricted by  $-0.4 \text{ GeV}^2 \geq -(t - t_0) \geq -0.1 \text{ GeV}^2$ , where  $t_0$  is the magnitude of the minimum squared momentum transfer to the nucleon. The exclusive nature of the reaction was maximized by requiring that the ratio  $z$  of the energy of the observed  $\rho^0$  meson to that of the virtual photon varies between 0.9 and 1.0. The variation of  $Q^2$  was between 0.7 and  $3.2 \text{ GeV}^2$ . The photon energy  $\nu$  varies from 2.2 to 4.8 GeV for  $Q^2$  between 0.7 and  $1.5 \text{ GeV}^2$  and from 2.4 to 4.6 GeV for  $Q^2$  values greater than  $1.5 \text{ GeV}^2$ . These kinematics correspond to a range of conventionally defined coherence lengths  $l_c \equiv 2\nu/(Q^2 + M_\rho^2)$  between 0.4 and 0.9 fm, which are larger than  $l_{in}$ . The localization of the interaction occurs between the narrow range between  $-l_{in}$  and  $l_{in}$ . Thus, we may safely take the start of the space time evolution of the virtual photon to occur at the nucleon center. The experimental kinematics are defined in terms of  $l_c$  [29], so we present our results as a function of  $l_c$ .

Sect. II is concerned with general issues of the reaction theory for nuclear electroproduction of vector mesons. The specific nature of the kinematics provides the motivation for Sect. III which develops the theory necessary to account for these kinematic restrictions. In particular, we derive a treatment of the energy lost by the rho in each step of multiple-scattering that also accounts for the momentum transfer to the nucleus. This, done using standard Glauber theory, is the main difference between the present effort and earlier ones such as [30]. We study the kinematics of the escaping ejectile as a function of the order of term in the multiple scattering series. The generalization to include the effects of color transparency is presented in Sect. IV. A brief summary is presented in Sect. V

## II. GENERAL ISSUES

### A. Basics

It is worthwhile to discuss color transparency for vector meson production from the perspective of high energies. The basic idea is that the incident virtual photon decays spontaneously into a  $q\bar{q}$  pair which then interacts strongly with the target system. At high energies where the space-time evolution of small wave packets is slow one can introduce a notion of the cross section of scattering of a small dipole configuration (say  $q\bar{q}$ ) of transverse size  $d$  on the nucleon [13, 31] which in the leading log approximation is given by [32]

$$\sigma(d, x_N) = \frac{\pi^2}{3} \alpha_s(Q_{eff}^2) d^2 [xG_N(x, Q_{eff}^2) + 2/3xS_N(x, Q_{eff}^2)], \quad (1)$$

where  $Q_{eff}^2 = \lambda/d^2$ ,  $\lambda = 4 \div 10$ ,  $x = Q_{eff}^2/s$ , with  $s$  the invariant energy of the dipole-nucleon system, and  $S$  is the sea quark distribution for quarks making up the dipole. The difference between Eq. (1) and the simplest two gluon exchange model [33] of this interaction is small, but grows as the energies increases.

For hard, high-energy processes in which a small dipole is produced (pion diffraction into two jets) or the initial state is highly localized (exclusive production of mesons for large

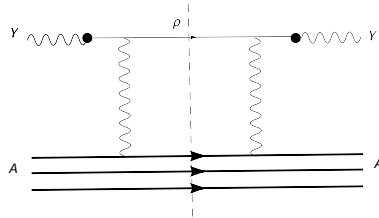


FIG. 1: Feynman diagram for the cross section. The vertical wiggly lines represent schematically the interaction of Eq. (1). The portion to the right of the dashed line represents the scattering amplitude and the portion to the left represents the complex conjugate of the scattering amplitude.

values of  $Q^2$ ), one can prove factorization theorems which allow the scattering amplitude to be represented as the product of the generalized parton densities, and wave functions in the frame in which the target is at rest and the projectile and the final system have high momentum[13, 32, 34, 35]. The proofs require the color transparency property in pQCD, understood in the sense of the suppression,  $\propto d^2$ , of multiple interactions of the dipole. Note that the definition of color transparency does not simply correspond to the nuclear amplitude being  $A$  times the nucleonic amplitude because both  $G_N$  and  $S_N$  may depend upon the nuclear environment. Instead, color transparency corresponds to the dominance of the leading twist term in the relevant scattering amplitude [13].

For vector meson production both quark  $\propto S_N$  and gluon  $\propto G_N$  exchanges are allowed. In pion production only exchange by a  $q\bar{q}$  pair is allowed. At Jlab kinematics, corresponding to  $x \geq 0.2$ , Eq. (1) is dominated by the quark contribution, and mechanism dominates the production of vector meson. We also note that pion production occurs via the knockout of a  $q\bar{q}$  pair. The kinematics are that of the ERBL region.

## B. Reaction Theory

We start our analysis of the nuclear reaction by considering the relevant Feynman diagrams for the  $\rho$ -meson production cross section. There are two classes of diagrams. One is corresponding to the quasi-classical picture in which  $\rho$  meson scatters from the same nucleons in both the *in* and *out* states, Fig. 1. We apply this picture for kinematics such that the struck nucleon is knocked out of the nucleus. If  $-t \geq 6/R_A^2$ , the square of the elastic nuclear (of radius  $R_A$ ) form factor will be very small, so that terms in which the nucleus remains in its ground state are absent. This condition is satisfied for the Jlab kinematics.

The second class includes all other diagrams which correspond to interference of interaction with different nucleons. The simplest two of them are shown in Fig. 2 and Fig. 3. The simplest one (Fig. 2) was considered in [32]. In contrast with the diagram of Fig. 1, these terms involve the two-nucleon correlation function, which in momentum space, is approximately proportional to the square of the nuclear form factor,  $F_A(t)^2$ . Thus these terms are substantially suppressed. For the region of  $t$  relevant for the Jlab experiments one can safely neglect the diagrams of the second kind.

Therefore we may organize the calculation in the following way. The production of the  $\rho$

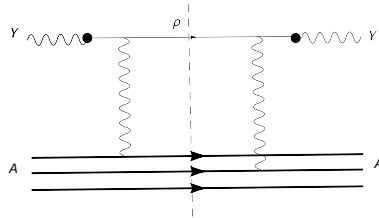


FIG. 2: Feynman diagram for the cross section. The vertical wiggly lines represent schematically the interaction of Eq. (1). The portion to the right of the dashed line represents the scattering amplitude and the portion to the left represents the complex conjugate of the scattering amplitude.

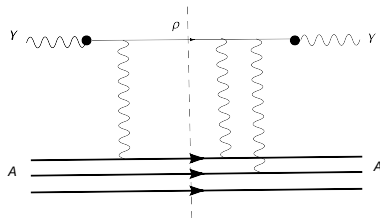


FIG. 3: Suppressed Feynman diagram for the cross section. The portion to the right of the dashed line represents the scattering amplitude and the portion to the left represents the complex conjugate of the scattering amplitude.

takes place on a given nucleon, and rescattering on other nucleons are expected to vanish if color transparency holds.

The transparency  $T_A$  is defined here as the ratio of the observed cross section to  $A$  (the nucleon number) times the cross section on a free nucleon, with perfect transparency occurring for  $T_A \rightarrow 1$ . Thus we start with the notation for the the rho meson production cross section on a single nucleon,  $\frac{d\sigma^{\gamma*}}{dt}$ :

$$\frac{d\sigma^{\gamma*}}{dt} = \left( \frac{d\sigma^{\gamma*}}{dt} \right)_{t=t_0} \exp(-B_1 q^2), \quad (2)$$

where the transverse momentum transfer variable  $q^2 \equiv \mathbf{q}^2 = -t$  ( $\mathbf{q}$  is in the  $\perp$  direction) and  $t_0$  corresponds to the minimum momentum transfer to the nucleon. The produced  $\rho$  then can interact with nucleons as it makes its way out of the nucleus. The  $\rho$ -nucleon scattering cross section is given by  $\frac{d\sigma^V}{dt}$  with

$$\frac{d\sigma^V}{dt} = \left( \frac{d\sigma^V}{dt} \right)_{t=0} \exp(-B_2 q_{\perp}^2). \quad (3)$$

in the  $t$ -range relevant for the JLab CT experiment. The total vector meson-nucleon cross section is denoted as  $\sigma_{\text{tot}}$ . It is traditional [36] to assume that this cross section is the same as that for pions. One could use the Particle Data Group parameterization [37] for the pion cross sections. However, the accuracy of this assumption has not been quantitatively tested, so we

TABLE I: Values of parameters used in the calculation.

$(\frac{d\sigma^{\gamma^*}}{dt})_{t=t_0}$ mb GeV <sup>-2</sup>	$B_1$ GeV <sup>-2</sup>	$\sigma_{\text{tot}}$ mb	$B_2 = B_{\text{soft}}$ GeV <sup>-2</sup>	$B_{\text{hard}}$ GeV <sup>-2</sup>	$R, a$ fm
1.25 – 1.5	6	25	6	2-4	1.1,0.54

shall report results using a small range of values of  $\sigma_{\text{tot}}$  between 25 and 30 mb. A convenient parametrization of the vector meson-nucleon scattering cross section, based on unitarity is:

$$\frac{d\sigma^V}{dt} = \frac{\sigma_{\text{tot}}^2}{16\pi} (1 + \alpha^2) \exp(-B_2 q_{\perp}^2), \quad (4)$$

where  $\alpha$  is the ratio of the real to imaginary parts of the elastic scattering amplitude. Values of the parameters are given in Table I.

The nuclear rho production cross section  $\frac{d\sigma}{dt}$  results from the production of a  $\rho$  meson by a single nucleon, followed by elastic rescattering on the surrounding nucleons. We thus express  $\frac{d\sigma}{dt}$  as

$$\frac{d\sigma}{dt} = \sum_{n=0}^{\infty} \frac{d\sigma_n}{dt}, \quad (5)$$

where  $n$  denotes the number of elastic rescattering terms. We explicitly count the number of elastic rescattering terms to keep track of the energy loss and ensure that we match the experimental conditions. We assume that any contribution to the vector meson-nucleon *inelastic* cross section involves large enough energy loss to be cut out of the ANL experiment.

We define the transparency as

$$T_n \equiv \frac{\frac{d\sigma_n}{dt}}{A \frac{d\sigma^{\gamma^*}}{dt}} \quad (6)$$

$$T_A = \frac{\frac{d\sigma}{dt}}{A \frac{d\sigma^{\gamma^*}}{dt}} = \sum_{n=0}^{\infty} T_n. \quad (7)$$

### III. GLAUBER FORMULAE

In the absence of the effects of color transparency, one expects that Glauber theory would provide a reasonable description of the data. Thus this theory serves as our starting point.

If no elastic rescattering takes place, the cross section is given by

$$\frac{d\sigma_0}{dt} = A \frac{d\sigma^{\gamma^*}}{dt} \int d^2b \int_{-\infty}^{\infty} dz \rho(b, z) (1 - \sigma_{\text{tot}} T(b, z))^{A-1}, \quad (8)$$

$$T(b, z) \equiv \int_z^{\infty} dz' \rho(b, z'). \quad (9)$$

Here the nuclear density  $\rho(r) = \rho(b, z) = \rho(\sqrt{b^2 + z^2})$  is normalized to unity. We take for heavy nuclei

$$\rho(r) = \frac{\rho_0}{1 + e^{\frac{r-R}{a}}}, \quad (10)$$

with  $R = 1.1A^{1/3}$  fm, and  $a=0.54$  fm. Combining Eq. (9) with Eq. (7) yields

$$T_0 = \int d^2b \int_{-\infty}^{\infty} dz \rho(b, z) (1 - \sigma_{\text{tot}}T(b, z))^{A-1}. \quad (11)$$

If a single elastic rescattering of the rho meson occurs one obtains a contribution,  $\frac{d\sigma_1}{dt}$  with

$$\begin{aligned} \frac{d\sigma_1}{dt} = & A(A-1) \left( \frac{d\sigma^{\gamma*}}{dt} \right)_{t=t_0} \left( \frac{d\sigma^V}{dt} \right)_{t=t_0} \int d^2b \int_{-\infty}^{\infty} dz \rho(b, z) T(b, z) (1 - \sigma_{\text{tot}}T(b, z))^{A-2} \\ & \int \frac{d^2q_1}{\pi} \frac{d^2q_2}{\pi} e^{-B_1q_1^2 - B_2q_2^2} \delta^{(2)}(\mathbf{q}_1 + \mathbf{q}_2 - \mathbf{q}). \end{aligned} \quad (12)$$

The integral over  $q_1, q_2$  can be evaluated with the result

$$\int \frac{d^2q_1}{\pi} \frac{d^2q_2}{\pi} e^{-B_1q_1^2 - B_2q_2^2} \delta^{(2)}(\mathbf{q}_1 + \mathbf{q}_2 - \mathbf{q}) = \frac{1}{\pi(B_1+B_2)} \exp\left(-\frac{B_1B_2}{B_1+B_2}q^2\right). \quad (13)$$

There is a hundred MeV cutoff on the nuclear excitation energy. The single scattering term above leads to nuclear excitation energies less than that, so the cutoff is not effective in this term and does not enter here. Then

$$\begin{aligned} T_1 = & (A-1) \frac{1}{\pi(B_1+B_2)} \exp\left(\frac{B_1^2}{B_1+B_2}q^2\right) \frac{\sigma_{\text{tot}}^2}{16\pi} (1 + \alpha^2) \\ & \int d^2b \int_{-\infty}^{\infty} dz \rho(b, z) T(b, z) (1 - \sigma_{\text{tot}}T(b, z))^{A-2}. \end{aligned} \quad (14)$$

The double rescattering term  $\frac{d\sigma_2}{dt}$  is given by

$$\begin{aligned} \frac{d\sigma_2}{dt} = & A(A-1)(A-2) \left( \frac{d\sigma^{\gamma*}}{dt} \right)_{t=t_0} \left[ \left( \frac{d\sigma^V}{dt} \right)_{t=t_0} \right]^2 \\ & \int d^2b \int_{-\infty}^{\infty} dz \rho(b, z) \frac{1}{2} \int_z^{\infty} dz' \rho(b, z') \int_z^{\infty} dz_2 \rho(b, z_2) \\ & (1 - \sigma_{\text{tot}}T(b, z))^{A-3} \int \frac{d^2q_2}{\pi} \int \frac{d^2q_3}{\pi} e^{-B_1q_1^2 - B_2q_2^2 - B_2q_3^2} \delta^{(2)}(\mathbf{q}_1 + \mathbf{q}_2 + \mathbf{q}_3 - \mathbf{q}). \end{aligned} \quad (15)$$

This term can be simplified to

$$\begin{aligned} \frac{d\sigma_2}{dt} = & \frac{A(A-1)(A-2)}{2} \left( \frac{d\sigma^{\gamma*}}{dt} \right)_{t=t_0} \left[ \left( \frac{d\sigma^V}{dt} \right)_{t=t_0} \right]^2 \\ & \int d^2b \int_{-\infty}^{\infty} dz \rho(b, z) T^2(b, z) (1 - \sigma_{\text{tot}}T(b, z))^{A-3} \\ & \int \frac{d^2q_1}{\pi} \frac{d^2q_2}{\pi} \int \frac{d^2q_3}{\pi} e^{-B_1q_1^2 - B_2q_2^2 - B_2q_3^2} \delta^{(2)}(\mathbf{q}_1 + \mathbf{q}_2 + \mathbf{q}_3 - \mathbf{q}). \end{aligned} \quad (16)$$

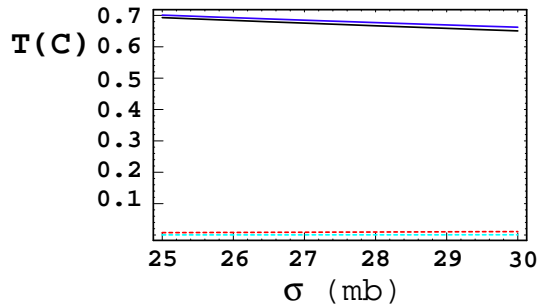


FIG. 4: (Color online) Glauber calculations for  $\rho$  production on  $C$ . Transparency *vs.*  $\sigma_{\text{tot}} = \sigma$ . The heavy solid (black) curve represents  $T_0$ , the long-dashed (red) curve  $T_1$ , and the short dashed (cyan) curve  $T_2$ . The sum  $T_0 + T_1 + T_2$  is shown as the solid thin (blue) curve. The forward limit, no transverse momentum transfer is used.

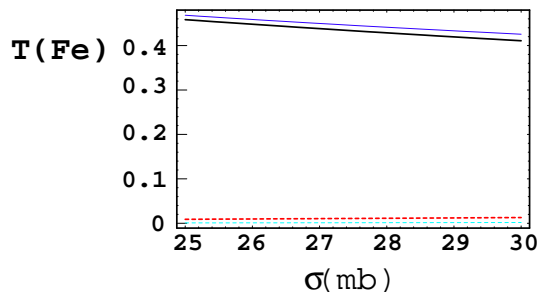


FIG. 5: (Color online) Glauber calculations for  $\rho$  production on  $Fe$ . Transparency *vs.*  $\sigma_{\text{tot}} = \sigma$ . The heavy solid (black) curve represents  $T_0$ , the long-dashed (red) curve  $T_1$ , and the short dashed (cyan) curve  $T_2$ . The sum  $T_0 + T_1 + T_2$  is shown as the solid thin (blue) curve. The forward limit, no transverse momentum transfer is used.

The result Eq. (16) is useful for the Glauber calculations, but Eq. (15) is more easily generalized to include the effects of color transparency. The integral over  $q_1, q_2, q_3$  can be done with the result

$$T_2 = \frac{2}{\pi B_2(4B_1 + B_2)} \exp\left(\frac{4B_1 B_2 q^2}{(4B_1 + B_2)}\right) \frac{(A-1)(A-2)}{2} \left[ \left( \frac{d\sigma^V}{dt} \right)_{t=t_0} \right]^2 \int d^2b \int_{-\infty}^{\infty} dz \rho(b, z) T^2(b, z) (1 - \sigma_{\text{tot}} T(b, z))^{A-3}. \quad (17)$$

Numerical results for the C and Fe targets are presented in Figs. 4 and 5. The effects of  $T_0$  are dominant. The limit of  $q^2 = 0$  is used here in evaluating Eq. (14) and Eq. (17). Using  $q^2 = 0.1 \text{ GeV}^2$ , (the value for which all contributions are largest) leads (for the  $Fe$  target) to enhancements of a 1.3 for  $T_1$  and 1.6 for  $T_2$ . These are not sufficient to modify the conclusion that the effects of  $T_0$  are dominant. These effects are much smaller for the carbon nucleus. Therefore we shall only be concerned with  $T_0$  in future sections on color transparency.



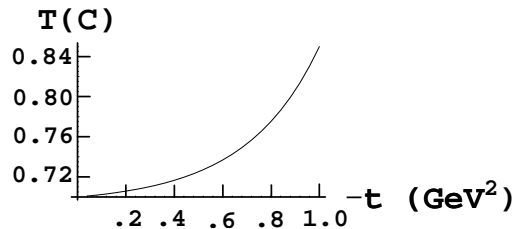


FIG. 6: Glauber calculations for  $\rho$  production on  $C$ . Transparency,  $T_0 + T_1 + T_2$ , vs.  $-(t - t_0)$ ,  $\sigma_{\text{tot}} = 25$  mb.

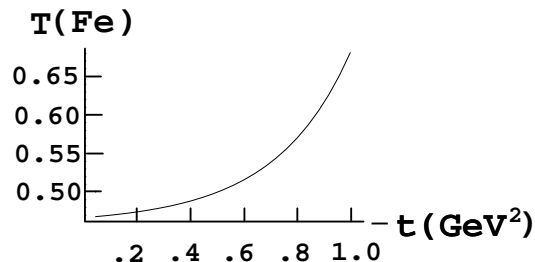


FIG. 7: Glauber calculations for  $\rho$  production on  $Fe$ . Transparency,  $T_0 + T_1 + T_2$ , vs.  $-(t - t_0)$ ,  $\sigma_{\text{tot}} = 25$  mb.

### A. Dependence on momentum transferred to the nucleus

So far we have taken  $\mathbf{q}^2 = 0$ . This factor appears in the equations Eq. (14), Eq. (17) for  $T_1, T_2$ . However, taking  $\mathbf{q}^2 \neq 0$  enhances both of these corrections to the leading term  $T_0$ . To illustrate the importance of controlling the kinematics, we display the total transparency,  $T = T_0 + T_1 + T_2$ , for  $^{12}\text{C}$  and  $^{56}\text{Fe}$  as a function of  $t$  in Figs. 6 and 7. One sees a rapid rise of  $T$  as  $-t$  increases. Experiments of resolution that effectively integrates over  $t$ , therefore observe a mix of transparencies. A change of acceptance in  $t$  that varies with the photon virtuality,  $Q^2$ , could mimic the turning on of color transparency. The theory of [38] presents  $t$ -integrated values of the transparency, obtained using a dipole expression for the  $q\bar{q}$  nucleon cross section that describes the DGLAP region quite well.

### B. Glauber Treatment of Rho Decay

We explain how the effects of  $\rho$  decay to  $\pi\pi$  are to be included in the calculations. This is to guide experimentalists in making the necessary corrections. The results of the previous sub-section are to be compared with experimental data which have been corrected for the effect. If the data have not been subject to this correction, this effect should be included.

The influence of  $\rho$  decay is implemented through the replacement

$$\sigma_{\text{tot}} T(b, z) \rightarrow \int_z^\infty dz' \rho(b, z') \hat{\sigma}(z' - z), \quad (18)$$

where

$$\widehat{\sigma}(z' - z) = \sigma_{\text{tot}} \exp \left[ -\frac{\Gamma m_\rho}{\sqrt{\nu^2 - m_\rho^2}} (z' - z) \right] + 2\sigma_{\pi N} \left( 1 - \exp \left[ -\frac{\Gamma m_\rho}{\sqrt{\nu^2 - m_\rho^2}} (z' - z) \right] \right). \quad (19)$$

The interpretation of this is that the produced vector meson state has two components,  $\rho$  and  $2\pi$  with a total probability of unity. As time goes by and  $z'$  increases from  $z$ , the  $\rho$  component decays away and the two pion component grows. In the limit that  $\nu \rightarrow \infty$ , one finds  $\sigma_{\text{eff}}(z' - z) \rightarrow \sigma_{\text{tot}}$ , which is the desired limit.

In the following, we make a simplified estimate using

$$\sigma_{\pi N} = \sigma_{\text{tot}}, \quad (20)$$

so that

$$\sigma_{\text{eff}}(z' - z) = \sigma_{\text{tot}} + \sigma_{\text{tot}} \left( 1 - \exp \left[ -\frac{\Gamma m_\rho}{\sqrt{\nu^2 - m_\rho^2}} (z' - z) \right] \right). \quad (21)$$

Again one can see that in the  $\nu \rightarrow \infty$  limit, the correction term vanishes. The effects of decay are to replace  $T(b, z)$  of Eq. (11) with  $T_D(b, z)$ , with

$$T_D(b, z) = T(b, z) + \int_z^\infty dz' \rho(b, z') \left( 1 - \exp \left[ -\frac{\Gamma m_\rho}{\sqrt{\nu^2 - m_\rho^2}} (z' - z) \right] \right) \quad (22)$$

Numerical results Figs. 8 and 9 show that this effect is about 5% at low  $\rho$  meson energies and much smaller at higher energies. The 5% rise should not be interpreted as being related to the onset of color transparency.

#### IV. COLOR TRANSPARENCY

This section is concerned with implementing the effects of color transparency. In the ideal situation of full color transparency one would simply neglect the effects of final state interactions and then one would find  $T_0=1$  under the assumption that the nuclear dependence of  $G_N, S_N$  may be neglected. However, for presently realistic experimental kinematics, the  $q\bar{q}$  pair is produced with a small, non-zero size, and expands as it moves through the nucleus. Therefore the effects of rescattering are expected to be considerable. Indeed, performing the experiment at increasing values of  $Q^2$  leads to producing  $\rho$  mesons of increasing energy, turning off effects of expansion and the related final state interactions. Observing this would amount to observing the onset of color transparency.

The physics of the expansion needs to be incorporated in realistic calculations. See the reviews [2, 3, 4, 7]. One technique is to express the putative PLC as a coherent superposition of hadronic states, such as in Jennings & Miller [10]. One may also use the quark-based treatment of Frankfurt & Strikman [39]. We use the latter which is more convenient, but the results of the two different formalisms are very similar [2]. The results Eq. (9), Eq. (12)

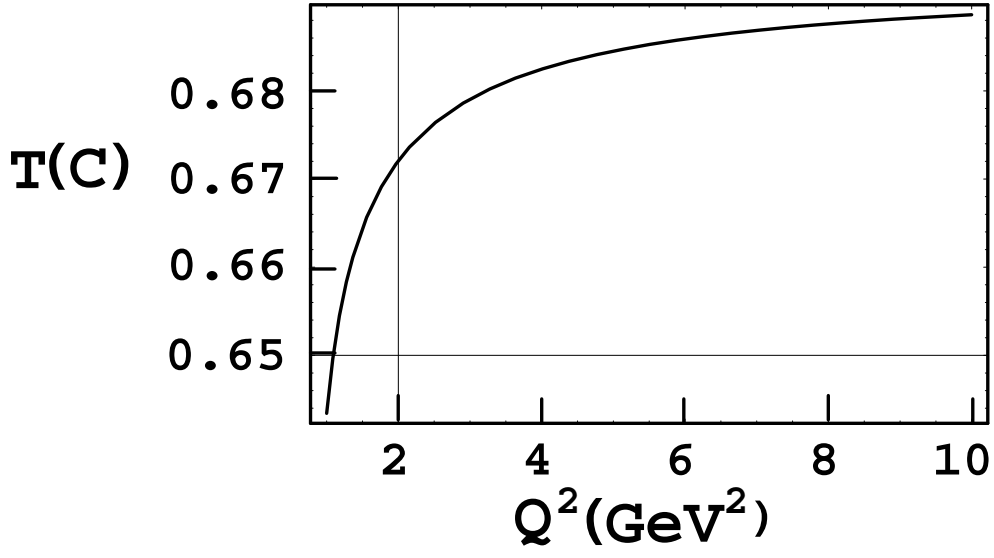


FIG. 8: Glauber calculations for  $\rho$  production on  $^{12}\text{C}$ , including the effects of rho decay on  $T_0$ . Transparency *vs.*  $\rho$  meson energy,  $\nu$ .

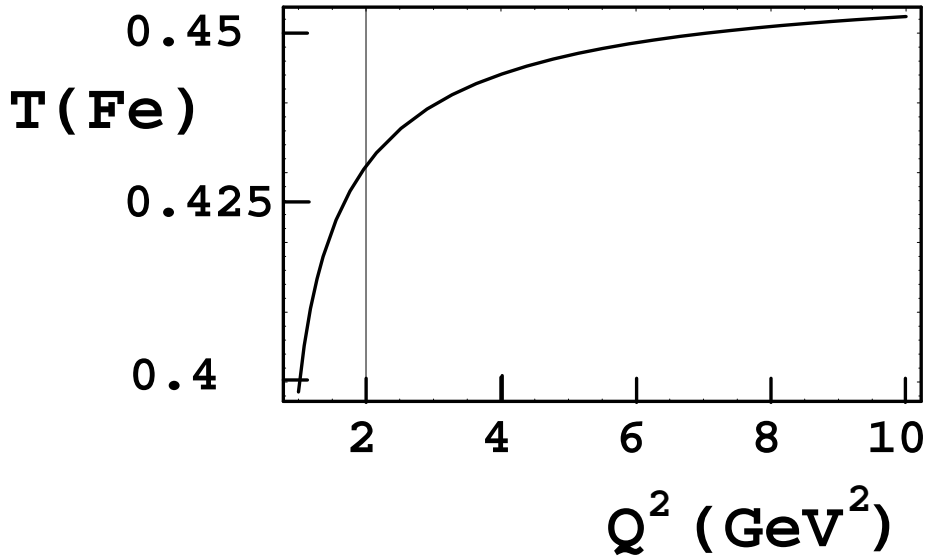


FIG. 9: Glauber calculations for  $\rho$  production on  $^{56}\text{Fe}$ , including the effects of rho decay on  $T_0$ . Transparency *vs.*  $\rho$  meson energy,  $\nu$ .

and Eq. (15) need to be modified. In those expressions the total cross section is replaced by an effective cross section,  $\sigma_{eff}$ , which takes the changing size of the ejectile into account. The effective interaction contains two parts, one for a propagation distance  $z' - z$  less than a length  $l_h$  describing the interaction of the expanding PLC, another, for larger values of  $z' - z$  describing the final state interaction of the physical particle. We use the expression [39]

$$\sigma_{\text{eff}}(z, p_\rho) = \sigma_{\text{tot}}(p_\rho) \left[ \left( \frac{n^2 \langle k_t^2 \rangle}{Q^2} + \frac{z}{l_h} \left( 1 - \frac{n^2 \langle k_t^2 \rangle}{Q^2} \right) \right) \theta(l_h - z) + \theta(z - l_h) \right], \quad (23)$$

where  $l_h = 2p_\rho/\Delta M^2$ , with  $\Delta M^2 = 0.7\text{GeV}^2$ . The prediction that the interaction of the PLC will be approximately proportional to the propagation distance  $z$  for  $z < l_h$  is called the quantum diffusion model.  $n^2 \langle k_t^2 \rangle / Q^2$ . In Eq. (23) the term

$$\sigma_{PLC} \equiv \sigma_{\text{tot}}(p_\rho) \frac{n^2 \langle k_t^2 \rangle}{Q^2} \quad (24)$$

is the cross section for the initially-produced PLC with  $n = 2$  and  $\langle k_t^2 \rangle^{1/2} \simeq 0.35$  GeV.

The coherence length,  $l_h$  sets the time scale for the PLC to evolve and determines the probability that a particle experiences reduced PLC interactions before leaving the nuclear matter. For propagation distances  $z > l_h$  the PLC interaction is that of a standard final state interaction with  $\sigma_{\text{eff}} \simeq \sigma_{\text{tot}}(p_\rho)$ , and is that of a typical Glauber-like calculation. In the limit  $l_h = 0$  a PLC is not created and the calculation reduces to a Glauber-like calculation.

We also include the effects of  $\rho$  decay into  $\pi\pi$  in the medium. These also modify color transparency as well as the Glauber calculation. Suppose the  $\rho$  has a width  $\Gamma = (149 \text{ MeV})$  [37], and has a Lorentz factor  $\gamma = E_\rho/m_\rho$ . Then, assuming the two pions have approximately equal momenta, Eq. (23) is modified to

$$\begin{aligned} \sigma_{\text{eff}}^D(z, p_\rho) = \sigma_{\text{tot}}(p_\rho) & \left[ \left( \frac{n^2 \langle k_t^2 \rangle}{Q^2} + \frac{z}{l_h} \left( 1 - \frac{n^2 \langle k_t^2 \rangle}{Q^2} \right) \right) \theta(l_h - z) + \theta(z - l_h) \exp\left(\frac{-\Gamma}{\gamma} z\right) \right] \\ & + 2\sigma_{\text{tot}}(\pi N)(p_\rho/2)\theta(z - l_h)(1 - \exp\left(\frac{-\Gamma}{\gamma} z\right)), \end{aligned} \quad (25)$$

where  $n = 2$ .

The effects of CT change the result Eq. (11) to

$$T_0 = \int d^2b \int_{-\infty}^{\infty} dz \rho(b, z) (1 - \sigma_{\text{tot}} T_{CT}(b, z, \nu, Q^2))^{A-1}, \quad (26)$$

with

$$T_{CT}(b, z, \nu, Q^2) = \int_z^\infty dz' \rho(b, z') \sigma_{\text{eff}}(z' - z, p_\rho) / \sigma_{\text{tot}} \quad (27)$$

or

$$T_0^D = \int d^2b \int_{-\infty}^{\infty} dz \rho(b, z) (1 - \sigma_{\text{tot}} T_{CT}^D(b, z, \nu, Q^2))^{A-1}, \quad (28)$$

with

$$T_{CT}^D(b, z, \nu, Q^2) = \int_z^\infty dz' \rho(b, z') \sigma_{\text{eff}}^D(z' - z, p_\rho) / \sigma_{\text{tot}} \quad (29)$$

The elastic scattering cross section could be substantially modified when the effects of color transparency are included. The expression Eq. (4) becomes

$$\frac{d\sigma_{CT}^V}{dt} = \frac{\sigma_{\text{eff}}(z, p_\rho)^2}{16\pi} (1 + \alpha^2) \exp(-B_2^{\text{CT}} q_\perp^2), \quad (30)$$

where  $B_2^{\text{CT}}$  depends on the propagation length  $z$  as:

$$B_2^{\text{CT}}(z) = (B_{\text{hard}} + (B_{\text{soft}} - B_{\text{hard}}) \frac{z}{l_c} \Theta(l_c - z) + B_{\text{soft}} \Theta(-l_c + z)) \quad (31)$$

This is based on the assumption that  $B_2$  is a radius squared that comes from the nucleon and the rho. The nucleon moves with low momentum here so its size is not modified by the effects color transparency, but the  $\rho$  is produced at high momentum transfer. Its effective radius is small (before the influence of expansion) but increases as the PLC moves.

In our calculations we shall be concerned with the leading terms of Eq. (26) and Eq. (28), taking the single nucleon  $\rho$  production cross section to be independent of the nuclear environment. The effects of Eq. (30) enter into the higher order terms that are negligible.

## A. Results

Figure 10 shows the effects of color transparency as a function of  $Q^2$  on a  $^{12}\text{C}$  target using a  $\rho - N$  cross section of 25 mb. Results for two different values of the coherence length  $l_c = \frac{2\nu}{(M_\rho^2 + Q^2)}$ , which determines  $\nu$  and the rho meson momentum, are shown. Figure 11 shows the effects of color transparency on a  $^{12}\text{C}$  target using a  $\rho - N$  cross section of 30 mb. We see that the effects of color transparency are expected to be substantial if one is able to measure the cross section at large enough values of  $Q^2$ . Increasing the value of  $l_c$  for a fixed value of  $Q^2$  increases the rho meson momentum and therefore increases the transparency. Figure 12 shows the effects of increasing the value of  $\Delta M^2$  from 0.7 to 0.8  $\text{GeV}^2$ . There is only a negligible effect, except for  $Q^2 \approx 10 \text{ GeV}^2$ . Figs. 13 and 14 display the effects of including the effects of rho meson decay. These can be substantial at low values of  $Q^2$  if the  $\rho N$  cross section is not too large.

Figure 15 shows the effects of color transparency as a function of  $Q^2$  on a  $^{56}\text{Fe}$  target using a  $\rho - N$  cross section of 25 mb. Results for two different values of the coherence length  $l_c = \frac{2\nu}{(M_\rho^2 + Q^2)}$ , which determines  $\nu$  and the rho meson momentum, are shown, and there is a substantial difference. Figure 16 shows the effects of color transparency on a  $^{56}\text{Fe}$  target using a  $\rho - N$  cross section of 30 mb. Again, we see that the effects of color transparency are expected to be substantial if one is able to measure the cross section at large enough values of  $Q^2$ . Increasing the value of  $l_c$  for a fixed value of  $Q^2$  increases the rho meson momentum and therefore increases the transparency. Figure 17 shows the effects of increasing the value of

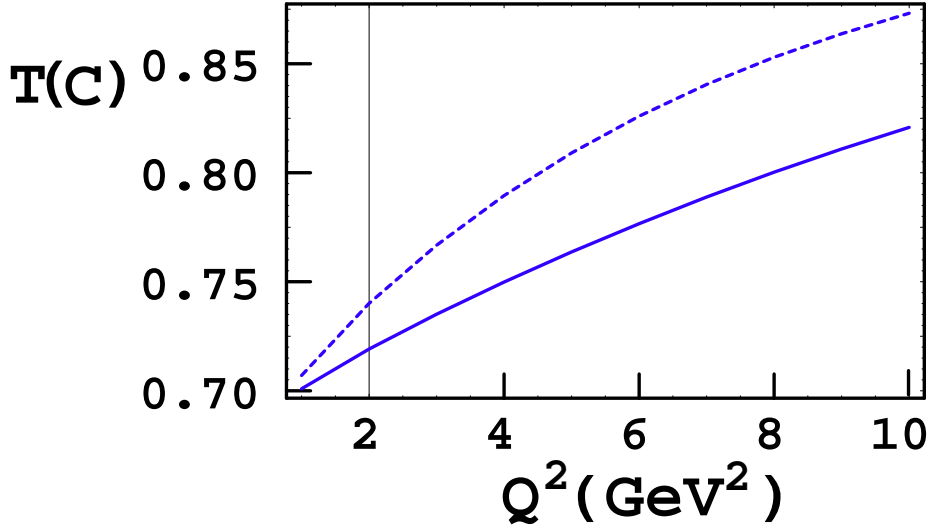


FIG. 10: (Color online)  $^{12}\text{C}$  Color transparency as a function of  $Q^2$  using  $T_0$  of Eq. (26) and Eq. (23) with  $\sigma_{\text{tot}} = 25$  mb. The upper dashed curve is computed using  $l_c = \frac{2\nu}{(M_p^2 + Q^2)} = 0.85$  fm. The lower solid curve is computed using  $l_c = 0.45$  fm.

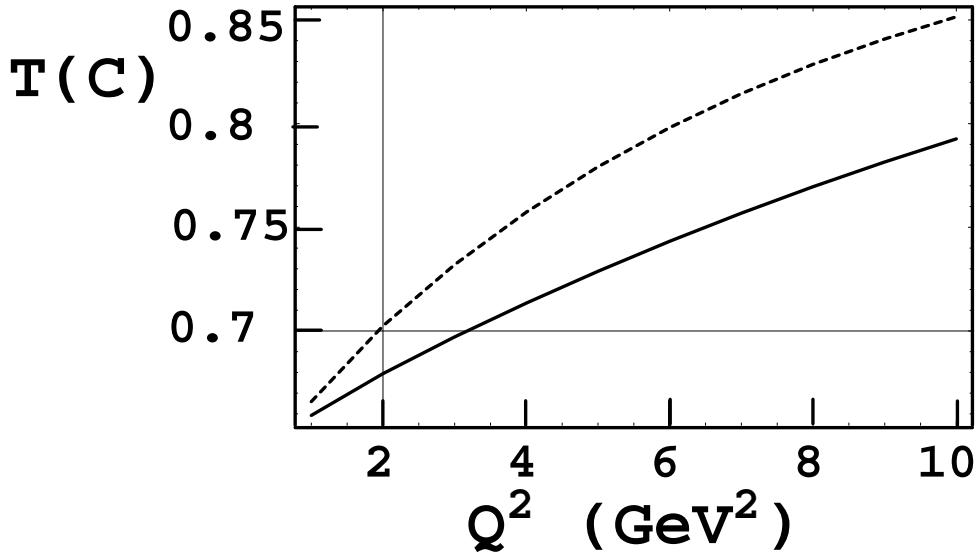


FIG. 11:  $^{12}\text{C}$  Color transparency according to Eq. (26) and Eq. (23). Here  $\sigma_{\text{tot}} = 30$  mb. The upper dashed curve is computed using  $l_c = \frac{2\nu}{(M_p^2 + Q^2)} = 0.85$  fm. The lower solid curve is computed using  $l_c = 0.45$  fm.

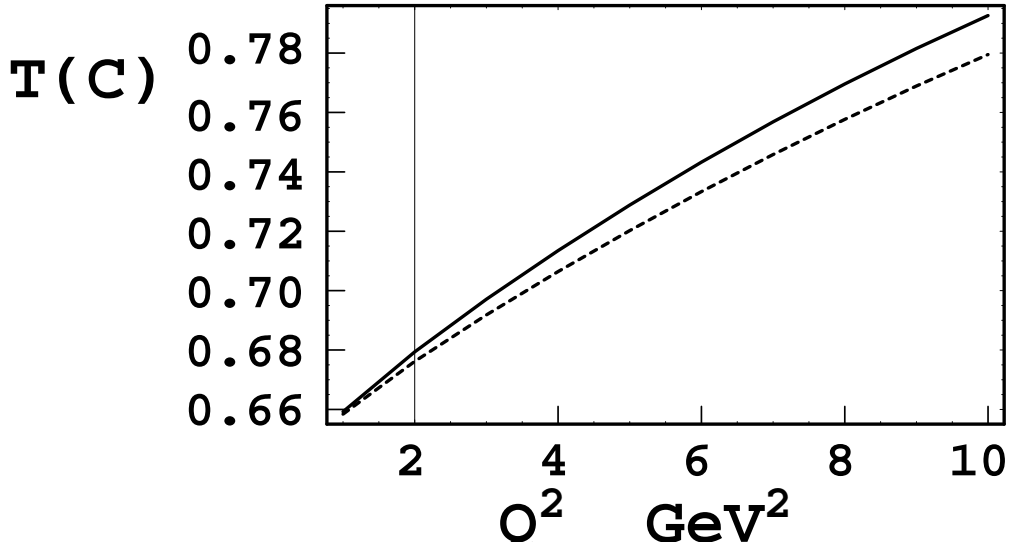


FIG. 12:  $^{12}\text{C}$  Color transparency according to Eq. (26) and Eq. (23). Here  $\sigma_{\text{tot}} = 30$  mb and  $l_c = \frac{2\nu}{(M_\rho^2 + Q^2)} = 0.85$  fm. The upper solid curve is computed using the standard value of  $\Delta M^2 = 0.7$   $\text{GeV}^2$ , and the lower dashed curve is computed using  $\Delta M^2 = 0.8$   $\text{GeV}^2$ .

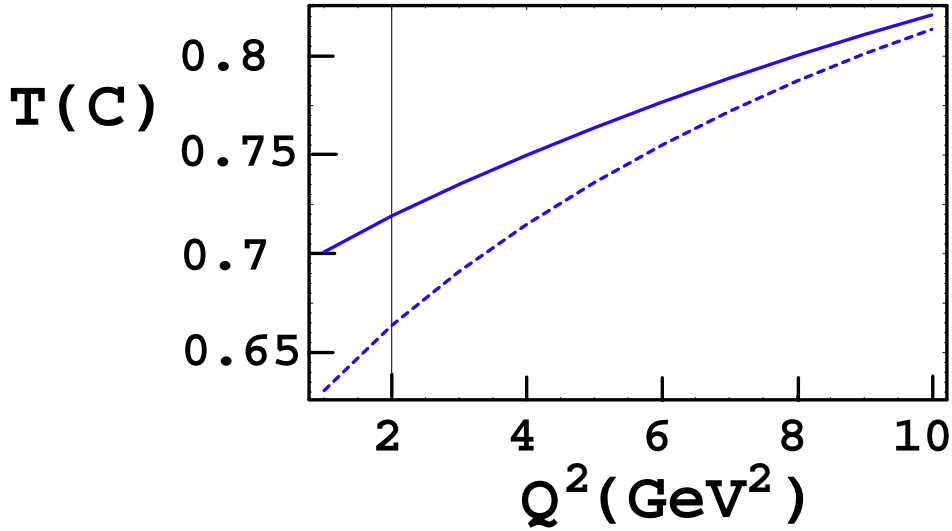


FIG. 13: (Color online) Effects of  $\rho$  meson decay on  $^{12}\text{C}$ . The parameters  $l_c = 0.45$  fm, and  $\sigma_{\text{tot}} = 25$  mb. The upper solid curve is computed using the effects of color transparency using  $T_0$  of Eq. (28) and Eq. (23). The lower dashed curve represents color transparency as modified by the use of Eq. (25) instead of Eq. (23).

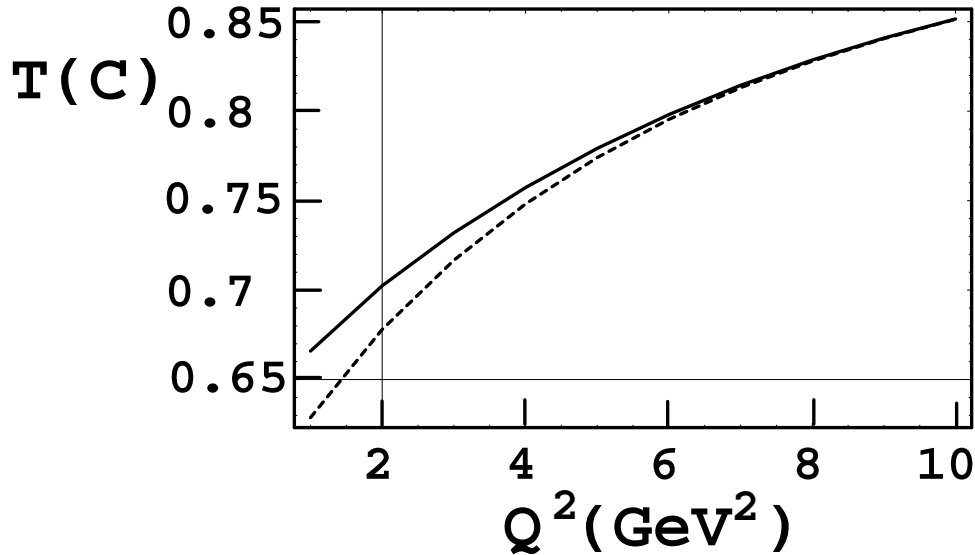


FIG. 14: Effects of  $\rho$  meson decay on  $^{12}\text{C}$ . The parameters  $l_c = 0.85$  fm, and  $\sigma_{\text{tot}} = 30$  mb. The upper solid curve is computed using the effects of color transparency using  $T_0$  of Eq. (26) and Eq. (23). The lower dashed curve represents color transparency as modified by the use of Eq. (25) instead of Eq. (23).

$\Delta M^2$  from 0.7 to 0.8  $\text{GeV}^2$ . Again there is only a negligible effect, except for  $Q^2 \approx 10$   $\text{GeV}^2$ . Figs. 18 and 19 display the effects of including the effects of rho meson decay. These can be substantial at low values of  $Q^2$  if the  $\rho N$  cross section is less than about 30 mb.

## V. SUMMARY

This work provides a reaction theory for electroproduction of vector mesons, for  $-t \gg 1/R_A^2$ , that allows one to assess the energy loss of each term in the multiple scattering series. These values of  $-t$  are sufficient to justify our semi-classical picture. We find however, that the leading term  $T_0$  of Eq. (11) and Eq. (26), Eq. (28) dominate for nuclei up to Fe, as long as the momentum transfer  $-t$  to the nucleus is sufficiently small. Higher-order terms in the multiple scattering series become important, causing a significant increase in the transparency as the value of  $-t$  increases. This effect, entering in Glauber theory, could mimic a signal of color transparency if the experimental acceptance in  $-t$  increases with the virtuality  $Q^2$  of the photon. We also study the effects of  $\rho$  meson decay inside the nucleus. These are typically about 5%, as long as the momentum transfer  $-t$  to the nucleus is small. This is large enough to influence the interpretation of the onset of color transparency. In particular, this effect disappears rapidly as  $Q^2$  increases from about 1 to 3  $\text{GeV}^2$ , causing a rise in the transparency that can not be interpreted as being related to color transparency.

We study the size of color transparency effects for C and Fe nuclei for values of  $Q^2$  up to



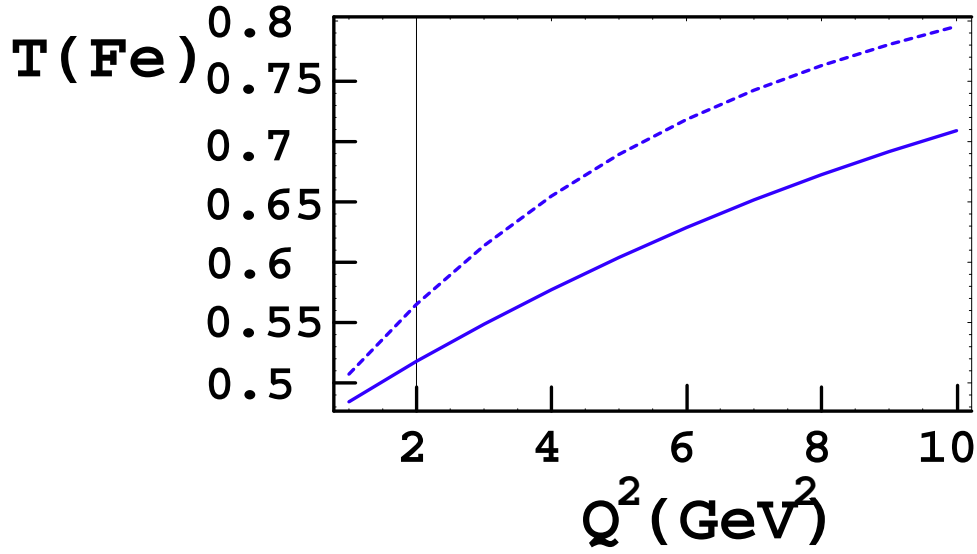


FIG. 15: (Color online)  $^{56}\text{Fe}$  Color transparency using  $T_0$  of Eq. (26) and Eq. (23) with  $\sigma_{\text{tot}} = 25$  mb. The upper dashed curve is computed using  $l_c = \frac{2\nu}{(M_p^2 + Q^2)} = 0.85$  fm. The lower solid curve is computed using  $l_c = 0.45$  fm.

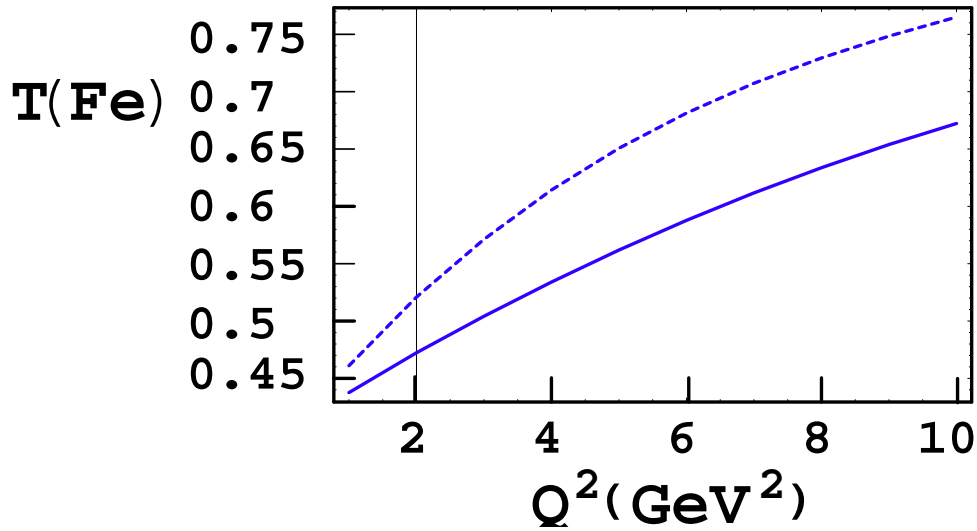


FIG. 16: (Color online)  $^{56}\text{Fe}$  Color transparency using  $T_0$  of Eq. (26) and Eq. (23) with  $\sigma_{\text{tot}} = 30$  mb. The upper dashed curve is computed using  $l_c = \frac{2\nu}{(M_p^2 + Q^2)} = 0.85$  fm. The lower solid curve is computed using  $l_c = 0.45$  fm.

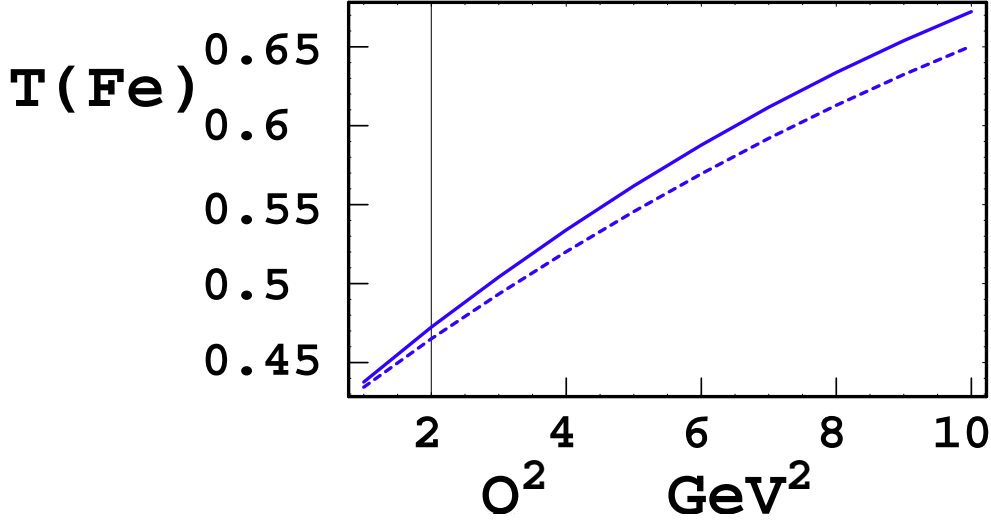


FIG. 17: (Color online)  $^{56}\text{Fe}$  color transparency according to Eq. (26) and Eq. (23). Here  $\sigma_{\text{tot}} = 30$  mb and  $l_c = \frac{2\nu}{(M_\rho^2 + Q^2)} = 0.85$  fm.. The upper solid curve is computed using the standard value of  $\Delta M^2 = 0.7$   $\text{GeV}^2$ , and the lower dashed curve is computed using  $\Delta M^2 = 0.8$   $\text{GeV}^2$ .

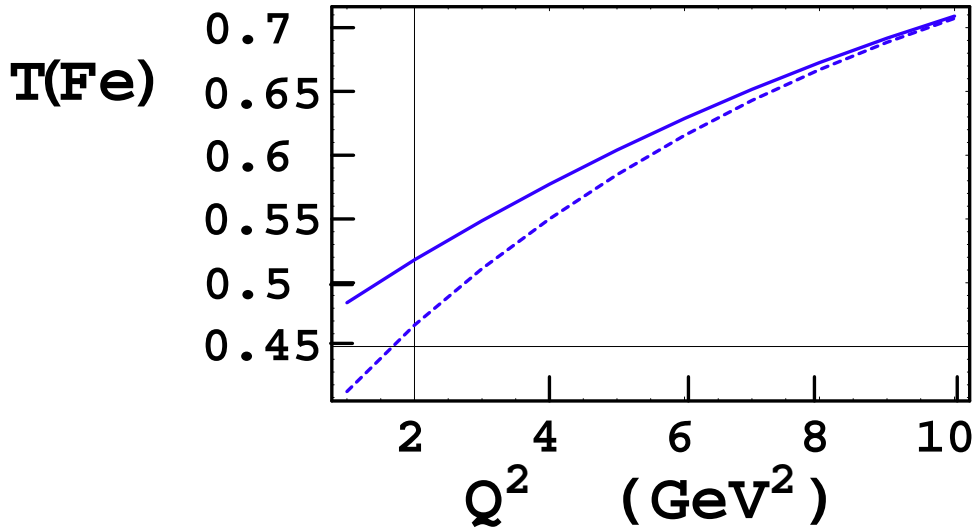


FIG. 18: (Color online) Effects of  $\rho$  meson decay on  $^{56}\text{Fe}$   $T_0$  using  $\sigma_{\text{tot}} = 25$  mb and  $l_c = 0.45$  fm. The upper solid curve is computed using Eq. (26) and Eq. (23) and the lower dashed curve is computed using using Eq. (26) and Eq. (25) to include the effects of decay.

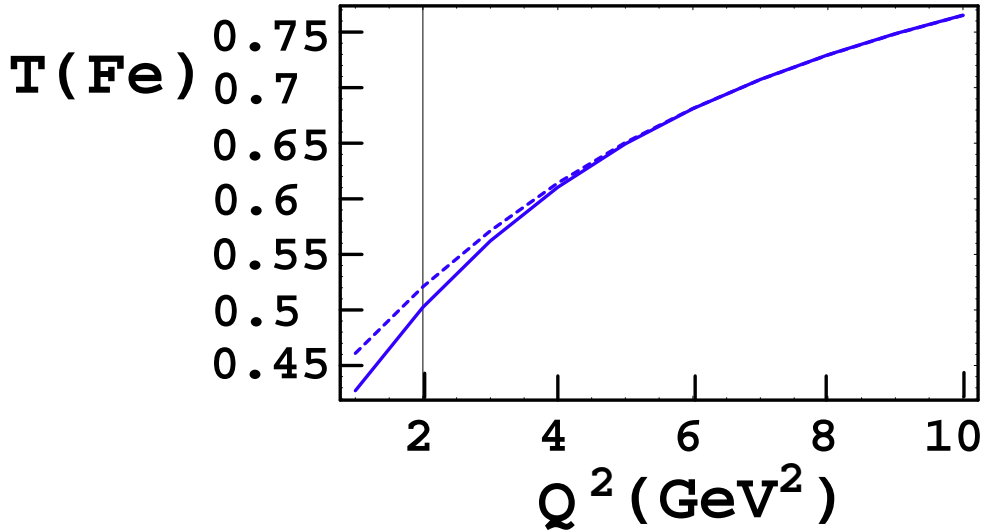


FIG. 19: (Color online) Effects of  $\rho$  meson decay on  $^{56}\text{Fe } T_0$  using  $\sigma_{\text{tot}} = 30$  mb and  $l_c = 0.45$  fm. The upper dashed curve is computed using Eq. (26) and Eq. (23) and the lower solid curve is computed using using Eq. (26) and Eq. (25) to include the effects of decay.

10  $\text{GeV}^2$ . The detailed results depend strongly on the assumed value of the  $\rho N$  cross section.

The overall effects of color transparency are large for both nuclear targets if  $Q^2$  is greater than about 5  $\text{GeV}^2$ . Testing our current theory, using the data of Ref.[29] will depend on the experimental ability to push the combined statistical and systematic errors for  $Q^2 \leq 3$   $\text{GeV}^2$  to better than about 10%.

### Acknowledgments

This research was supported by the the US Israeli BNSF (LF) and by the United States Department of Energy (GAM and MS). We thank K. Hafidi and L. El Fassi for useful discussions regarding their experiment.

- 
- [1] A.H. Mueller in Proceedings of Seventeenth Rencontre de Moriond, Les Arcs, 1982 ed. J Tran Thanh Van (Editions Frontieres, Gif-sur-Yvette, France, 1982) Vol. I, p13; S.J. Brodsky in Proceedings of the Thirteenth Int'l Symposium on Multiparticle Dynamics, ed. W. Kittel, W. Metzger and A. Stergiou (World Scientific, Singapore 1982,) p963.
  - [2] L. L. Frankfurt, G. A. Miller and M. Strikman, Ann. Rev. Nucl. Part. Sci. **44**, 501 (1994) [arXiv:hep-ph/9407274].

- [3] G. A. Miller, In *\*Close, Frank (ed.) et al.: Electromagnetic interactions and hadronic structure\** 457-494
- [4] L. Frankfurt and M. Strikman, Phys. Rep. **160**, 235, (1988).
- [5] F. E. Low, Phys. Rev. **D12**, 163 (1975); S. Nussinov, Phys. Rev. Lett **34**, 1286 (1975).
- [6] H.-N. Li and G. Sterman, Nucl. Phys. **B381**, 129 (1992); J. Botts and G. Sterman, Nucl. Phys. **B325**, (1989) 62.
- [7] L. Frankfurt, G.A. Miller, and M. Strikman, Comments Nucl. Part. Phys. **21**, 1 (1992).
- [8] L. Frankfurt, G.A. Miller, and M. Strikman, Nucl. Phys. **A555**,752 (1993).
- [9] G.R. Farrar, H. Liu, L.L. Frankfurt & M.I. Strikman, Phys. Rev. Lett. **61**, 686 (1988).
- [10] B.K. Jennings and G.A. Miller, Phys. Lett. **B236**, 209 (1990); B.K. Jennings and G.A. Miller, Phys. Rev. **D44**, 692 (1991); Phys. Rev. Lett. **69**, 3619 (1992); Phys. Lett. **B274**, 442 (1992).
- [11] S.J. Brodsky and A.H. Mueller, Phys. Lett. **B206**, 685 (1988).
- [12] E. M. Aitala *et al.* [E791 Collaboration], Phys. Rev. Lett. **86**, 4773 (2001).
- [13] L. Frankfurt, G. A. Miller and M. Strikman, *Phys. Lett.* **B304**, 1 (1993).
- [14] L. Frankfurt, G. A. Miller and M. Strikman, Found. Phys. **30**, 533 (2000) [arXiv:hep-ph/9907214]; L. Frankfurt, G. A. Miller and M. Strikman, Phys. Rev. D **65**, 094015 (2002) [arXiv:hep-ph/0010297].
- [15] M. D. Sokoloff *et al.* [Fermilab Tagged Photon Spectrometer Collaboration], Phys. Rev. Lett. **57**, 3003 (1986).
- [16] H. Abramowicz and A. Caldwell, Rev. Mod. Phys. **71**, 1275 (1999).
- [17] I. Mardor *et al.*, Phys. Rev. Lett. **81**,5085 (1998).
- [18] J. L. S. Aclander *et al.*, *Phys. Rev.* **C70**, 015208 (2004).
- [19] N.C.R. Makins *et al.*, Phys. Rev. Lett. **72**, 1986 (1994); T.G. O'Neill *et al.*, Phys. Lett **B351**, 87 (1995).
- [20] D. Abbott *et al.*, Phys. Rev. Lett. **80**, 5072 (1998).
- [21] S. J. Brodsky and G. F. de Teramond, Phys. Rev. Lett. **60**, 1924 (1988).
- [22] J. P. Ralston and B. Pire, Phys. Rev. Lett. **65**, 2343 (1990).
- [23] B. K. Jennings and G. A. Miller, Phys. Rev. D **44**, 692 (1991).
- [24] B. K. Jennings and G. A. Miller, Phys. Rev. Lett. **69**, 3619 (1992) [arXiv:hep-ph/9207211]; B. K. Jennings and G. A. Miller, Phys. Lett. B **318**, 7 (1993) [arXiv:hep-ph/9305317].
- [25] L. L. Frankfurt, M. I. Strikman and M. B. Zhalov, Phys. Rev. C **50**, 2189 (1994).
- [26] B. Clasio *et al.*, Phys. Rev. Lett. **99**, 242502 (2007)
- [27] A. Larson, G. A. Miller and M. Strikman, *Phys. Rev.* **C74**, 018201 (2006).
- [28] W. Cosyn, M. C. Martinez and J. Ryckebusch, Phys. Rev. C **77**, 034602 (2008)
- [29] K. Hafidi, and M. Holtrop, Jlab proposal PR-02-110
- [30] T. Falter, K. Gallmeister and U. Mosel, Phys. Rev. C **67**, 054606 (2003) [Erratum-ibid. C **68**, 019903 (2003)] [arXiv:nucl-th/0212107].
- [31] B. Blaettel, G. Baym, L. L. Frankfurt and M. Strikman, Phys. Rev. Lett. **70**, 896 (1993).
- [32] L. Frankfurt, G. A. Miller and M. Strikman, *Phys. Rev.* **D65**, 094015 (2002).
- [33] J. F. Gunion and D. E. Soper, *Phys. Rev.* **D15**, 2617 (1977).
- [34] S. J. Brodsky, L. Frankfurt, J. F. Gunion, A. H. Mueller and M. Strikman, *Phys. Rev.* **D50**, 3134 (1994).
- [35] J. C. Collins, L. Frankfurt and M. Strikman, *Phys. Rev.* **D56**, 2982 (1997).

- [36] T. H. Bauer, R. D. Spital, D. R. Yennie and F. M. Pipkin, *Rev. Mod. Phys.* **50**, 261 (1978)  
[Erratum-ibid. **51**, 407 (1979)].
- [37] S. Eidelman et al.[PDG], *Physics Letters B*592, 1 (2004)
- [38] B. Z. Kopeliovich, J. Nemchik, A. Schafer and A. V. Tarasov, *Phys. Rev. C* **65**, 035201 (2002).  
B. Z. Kopeliovich, J. Nemchik and I. Schmidt, *Phys. Rev. C* **76**, 015205 (2007).
- [39] G. R. Farrar, H. Liu, L. L. Frankfurt and M. I. Strikman, *Phys. Rev. Lett.* **61**, 686 (1988).